Available online at www.sciencedirect.com
SCIENCE DIRECT®
Tectonophysics 377 (2003) 179–196
TECTONOPHYSICS
www.elsevier.com/locate/tecto

Multicomponent magnetization in western Dolpo (Tethyan Himalaya, Nepal): tectonic implications

C. Crouzet[a], P. Gautam[a,b], E. Schill[a,c], E. Appel[a,*]

[a] *Institut für Geowissenschaften, Universität Tübingen, Sigwartstraße 10, 72076 Tübingen, Germany*
[b] *Central Department of Geology, Tribhuvan University, Kirtipur, Kathmandu, Nepal*
[c] *Institut für Geophysik, ETH-Hoenggerberg, HPP O14, 8093 Zürich, Switzerland*

Received 5 August 2002; received in revised form 28 February 2003; accepted 25 August 2003

Abstract

A palaeomagnetic study has been carried out in the Tethyan Himalaya (TH; the northern margin of Greater India). Twenty-six palaeomagnetic sites have been sampled in Triassic low-grade metasediments of western Dolpo. Two remanent components have been identified. A pyrrhotite component, characterized by unblocking temperatures of 270–335 °C, yields an in situ mean direction of $D=191.7°$, $I=-30.9°$ ($k=29.5$, $\alpha_{95}=5.7°$, $N=23$ sites). The component fails the fold test at the 99% confidence level ($k_{\text{in situ}}/k_{\text{bed}}=6.9$) and is therefore of postfolding origin. For reason of the low metamorphic grade, this pyrrhotite magnetization is believed to be of thermo-chemical origin. Geochronological data and inclination matching indicate an acquisition age around 35 Ma. The second remanence component has higher unblocking temperatures (>400 °C and up to 500–580 °C range) and resides in magnetite. A positive fold test and comparison with expected Triassic palaeomagnetic directions suggest a primary origin.

The postfolding character of the pyrrhotite component, and its interpreted age of remanence acquisition, implies that the main Himalayan folding is older than 35 Ma in the western Dolpo area. This study also suggests that the second metamorphic event (Neo-Himalayan) was more significant in the Dolpo area than the first (Eo-Himalayan) one.

A clockwise rotation of 10–15° is inferred from the pyrrhotite component, which is compatible with oroclinal bending and/or rotational underthrusting models. This rotation is also supported by the magnetite component, indicating that no rotation of the Tethyan Himalaya relative to India took place before 35 Ma.

Keywords: Tethyan Himalaya; Nepal; Palaeomagnetism; Rotation; Pyrrhotite; Magnetite

1. Introduction

Palaeomagnetism is an important tool for determination of rotational and translational motions during convergence of the Indian subcontinent with Eurasia prior to and after collision. The typical problems encountered in this respect are: (1) determining the age of secondary magnetization; (2) identification and separation of regional, mesoscale and local components of motions; and (3) quantification of the amounts of rotational underthrusting, oroclinal bending and large-scale tilting (Klootwijk and Bingham,

* Corresponding author.
E-mail address: erwin.appel@uni-tuebingen.de (E. Appel).

0040-1951/$ - see front matter © 2003 Elsevier B.V. All rights reserved.
doi:10.1016/j.tecto.2003.08.019

1980; Klootwijk et al., 1985, 1991; Appel et al., 1991, 1995; Rochette et al., 1994; Patzelt et al., 1996; Schill et al., 2001). The Dolpo area lies in the Tethyan Himalaya (TH), between palaeomagnetically studied areas of the western Himalaya (Appel et al., 1995; Schill et al., 2001, 2002b) and the central Himalaya (Klootwijk and Bingham, 1980; Appel et al., 1991; Crouzet et al., 2001b; Schill et al., 2002a; Schill et al., 2003, submitted for publication). The present study is therefore thought crucial for linking the available palaeomagnetic data set of the Tethyan Himalaya.

This paper deals with the analysis of remanent magnetizations residing in pyrrhotite and in magnetite. It provides constraints on timing of major Himalayan deformational and metamorphic events and on tectonic rotation in the western Dolpo area.

2. Geological setting

The TH, comprising the Tibetan Sedimentary Series (TSS), stretches all along the Himalayan arc and represents the deformed remnant of the passive northern edge of the Indian subcontinent (Garzanti, 1999). The Indus–Yarlung Suture Zone (IYSZ) in the north and the South Tibetan Detachment System (STDS) in the south tectonically bound the TH zone (Fig. 1). The sedimentary pile has a thickness of ~ 6–7 km and is made up of a fairly complete and well-preserved Cambro-Ordovician to Eocene succession (Bassoulet et al., 1980; Brookfield, 1993; Garzanti, 1999).

Following the collision between India and Asia in the Early Tertiary, the TSS was strongly tectonised. Lower Palaeozoic units form the backbone of the Annapurna and Dhaulagiri Massifs and lie tectonically above the Higher Himalayan Crystalline (HHC). The TSS has undergone polyphase deformation with folding and thrusting and very-low- to medium-grade metamorphism. This led to crustal thickening followed shortly by prograde regional metamorphism due to burial (Godin et al., 1999, 2001; Crouzet et al., 2001a).

The Dolpo–Manang Synclinorium (DMS) is the largest (>100 km) fold structure of the TH, with an exposed core of Triassic–Jurassic sediments (Figs. 1 and 2). According to Fuchs (1977), the synclinal cores commonly exhibit imbrications and faults that generally follow strike, indicating near synchronism with folding. In the Dolpo area, strata younger than Jurassic were eroded during the strong uplift of the latest few million years (Fuchs, 1967; Fuchs et al., 1988).

The age of metamorphism in TH is poorly constrained due to its low grade, but information on the tectonometamorphic evolution of the Himalayan belt can be deduced from the HHC. The HHC was subjected to two main phases of deformation and metamorphism known as Eo-Himalayan (M1) and Neo-Himalayan (M2). The M1 phase corresponds to a Barrovian type metamorphism affecting the HHC and lower part of TSS climaxing around the end of Eocene. The initial period of the high-grade M1 phase in Nepal is marked by Middle Eocene–Early Oligocene ages (36–35 Ma: Hodges et al., 1996; 35 ± 3 Ma: Godin et al., 1999). The M1 phase corresponding to the pressure peak with cooling ages of 40–30 Ma is attributed to crustal thickening (Guillot et al., 1999). This phase is linked with the formation of an Oligocene fan structure that has tectonically thickened the initial 6–7 km of the TSS to ~ 25 km. It caused a kyanite-grade melting at deeper structural levels, occurring between the initial collision (ca. 55–50 Ma) and the time of movement along the Main Central Thrust (MCT) at ca. 23–20 Ma (Vannay and Hodges, 1996; Godin et al., 1999). The Miocene M2 phase in the HHC corresponds to the temperature peak and was characterized by synmetamorphic uplift, doming and incipient anatexis. The metamorphic event was probably contemporaneous with MCT thrusting and synchronous with N–S extension along the STDS. The age of formation of the MCT may have varied along the Himalaya, but all existing quantitative constraints fall within a narrow time range of 23–20 Ma (Hodges, 2000, and references therein). However, evidence of M1 effects on the TH in the central Himalayan sector during the first stages of the Himalayan orogeny is scarce because of the advanced re-equilibration of metamorphic mineral assemblages that took place during Miocene (see Hodges, 2000 for a review). Most thermochronological data from the central Himalaya record cooling after intense M1 metamorphism and anatexis associated with tectonic transport along the MCT.

In the TH, the highest metamorphic temperatures and the highest intensity of deformation

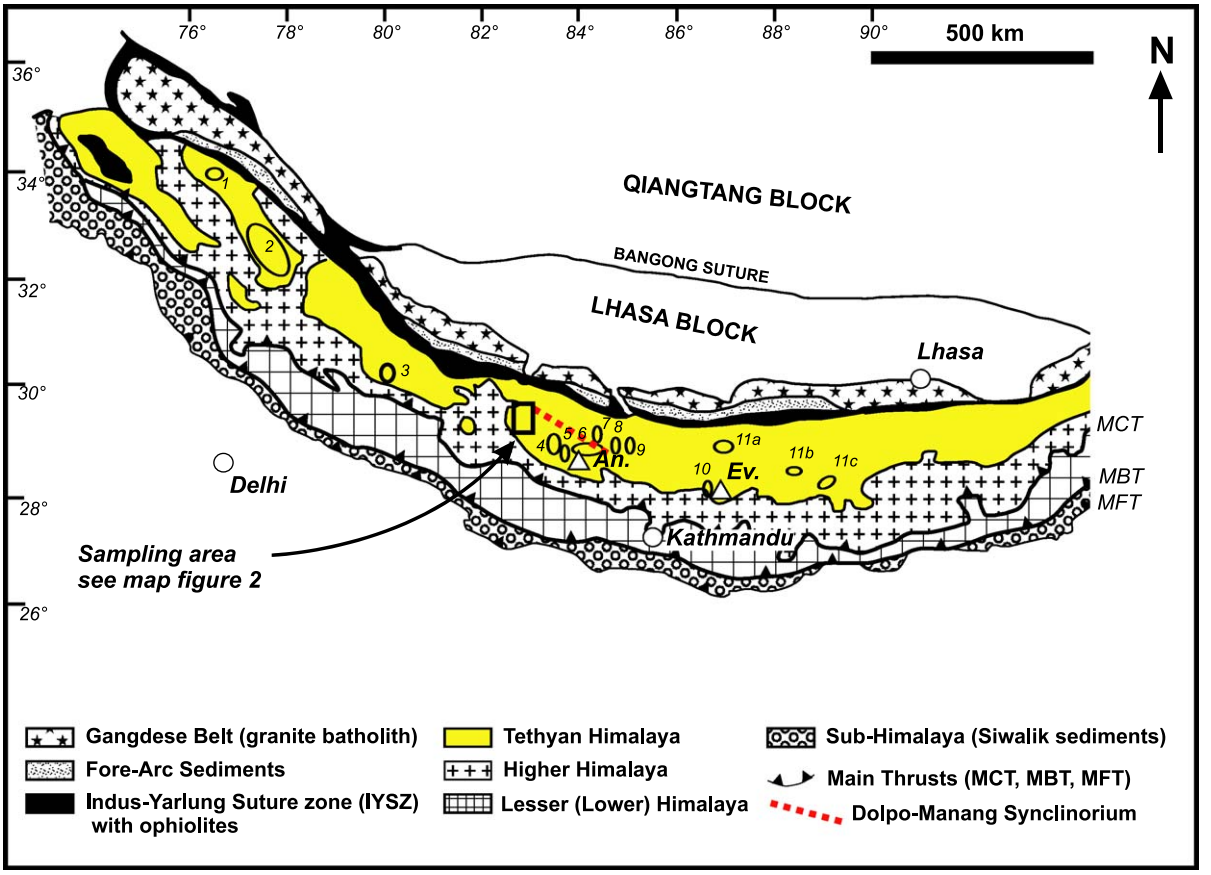

Fig. 1. Simplified geological map of the Himalayan belt (after Searle et al., 1987, modified). The rectangular box indicates the sampled area. Other palaeomagnetic studies in the Tethyan Himalaya are (1) NW Zanskar (Appel et al., 1995); (2) Sarchu, Lossar and Spiti (Schill et al., 2001); (3) Malari (Schill et al., 2002b); (4) Hidden Valley (Crouzet et al., 2001a,b); (5) Thakkhola (Klootwijk and Bingham, 1980); (6) Manang (Appel et al., 1991); (7) Nar-Phu (Schill et al., 2003); (8) Larkya (Schill et al., submitted); (9) Shiar Khola (Schill et al., 2002a); (10) Everest (Rochette et al., 1994); (11a) Tingri, (11b) Gamba, (11c) Duela (Patzelt et al., 1996).

occurred at the deepest structural levels of Cambrian–Ordovician limestone (Colchen et al., 1980; Schneider and Masch, 1993; Garzanti et al., 1994). Deformation intensity and metamorphic grade both decrease progressively northward from amphibolite facies in Early Palaeozoic metacarbonates to greenschist facies in the middle Palaeozoic sediments (Tilicho Pass Fm, central Dolpo). Mesozoic sediments have been less metamorphosed at pre-anchizonal grade and diagenesis (Garzanti et al., 1994).

Palaeotemperature estimates from the TH in the Dolpo area are scarce. Garzanti et al. (1994) and Crouzet et al. (2002a,b) have reported illite and chlorite ''crystallinity'' and vitrinite reflectance (VR) data from the Tarap area (central Dolpo) and the Shey Gompa area (western Dolpo), respectively. In the Tarap area, illite crystallinity (IC) data range from 0.44 to 0.50 in Triassic sediments and up to 0.25 in Devonian ones. The VR values vary between $R_{max} \sim 4.8$ and $R_{min} \sim 2.7$. Palaeotemperature estimates for the Triassic sediments using IC and VR yield 245–275 °C in the Tarap area. In the Shey Gompa area, IC values, for Triassic samples, are very similar to those from the Tarap area, while a slightly higher level of maturation is indicated by

the VR data. Crouzet et al. (2002a,b) have therefore concluded to palaeotemperatures between 250 and 300 °C.

The sampled area corresponds to a succession of SW verging folds with NE–SW axis. Locally, small thrusts and duplex structures are present (Fig. 2).

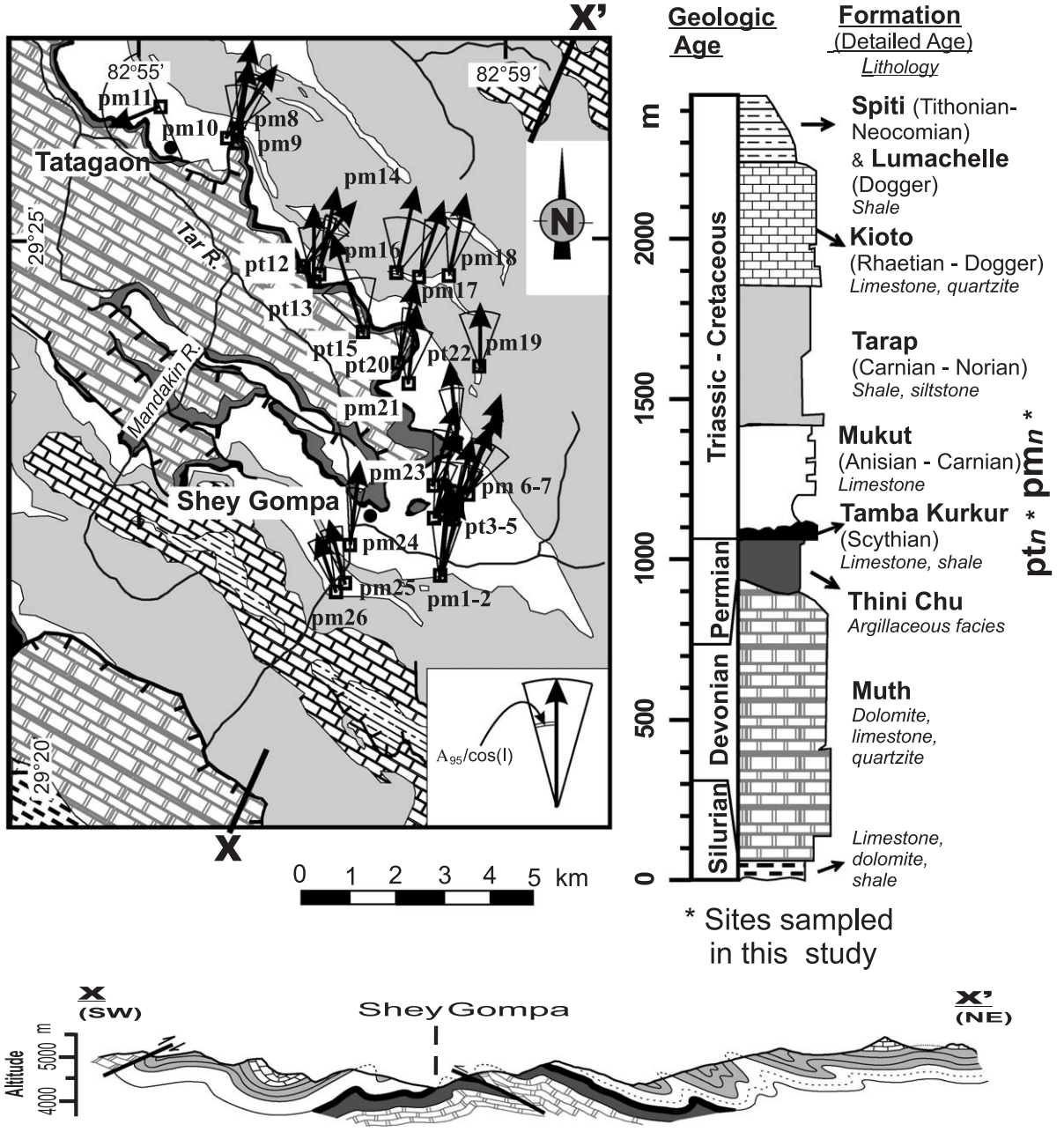

Fig. 2. Geological map, stratigraphic column and cross section of the study area in Dolpo (after Fuchs, 1977). Open squares: palaeomagnetic-sampling locations. The arrows indicate the declinations of the in situ pyrrhotite remanence (for data, see Table 1). Length of arrows is proportional to (90°−Ipyr).

3. Sampling and laboratory procedures

Twenty-six palaeomagnetic sites were sampled in 1999 from the Triassic Mukut and Tamba–Kurkur Formations (labelled respectively pm and pt) around and north of Shey Gompa (Fig. 2). The Mukut Formation (Anisian–Carnian or Aegean to Early Lacian after Garzanti, 1999) is made up of marly limestones and marls, while the Tamba–Kurkur Formation (Scythian or Griesbachian after Garzanti, 1999) is made up of pelagic limestones and shales. A portable gasoline-powered rock drill was used for taking cores of 2.5 cm in diameter, which were oriented in situ with a magnetic compass. No deviations in compass readings by strong local magnetic sources were observed. Generally, 10 cores (6–10 cm in length) were obtained from each site.

Standard specimens of 2.2–2.4 cm length were cut from these samples. The following instruments were used: a Kappabridge KLY-2 (Agico) for measuring anisotropy of susceptibility (AMS) and to monitor the bulk susceptibility after each heating step; a 755R SQUID magnetometer (2G Enterprises) with a noise level of ~ 0.005 mA m^{-1} (for 10-cm^3 samples) for remanence measurements; a static tri-axial demagnetizer (2G Enterprises) of 150 mT maximum field for alternating field demagnetization (AFD); a MMTD18 or MMTD60 furnace (Magnetic Measurements) for progressive thermal demagnetization (ThD); a MMPM9 pulse magnetizer (Magnetic Measurements) with 2.5 T maximum field to impart isothermal remanent magnetization (IRM); a fluxgate spinner magnetometer (Molspin) with a noise level ~ 0.2 mA m^{-1} (for 10-cm^3 samples) to measure IRM. Measurements were carried out at the palaeomagnetic laboratory of Tübingen University.

Prior to magnetic cleaning, the AMS was measured in order to detect a possible correlation between the rock magnetic fabric and the remanence direction. During pilot demagnetization, two specimens from each site were analysed. One specimen was subjected to stepwise ThD from 100 to 580 °C, generally with 50 °C steps, but steps of 20–30 °C were applied between 250 and 350 °C and close to 580 °C, which represent the unblocking temperatures (T_{ub}) ranges of pyrrhotite and magnetite, respectively. The other specimen was subjected to AFD up to 140 mT in 2–20 mT steps. The specimens treated with AFD were then imparted an IRM in fields up to 2.5 T, followed by ThD in 16 steps up to 700 °C. Based on the pilot results, mainly ThD was used to process the bulk of the specimens. In some cases, AFD was used after 400 °C heating step in order to avoid changes in

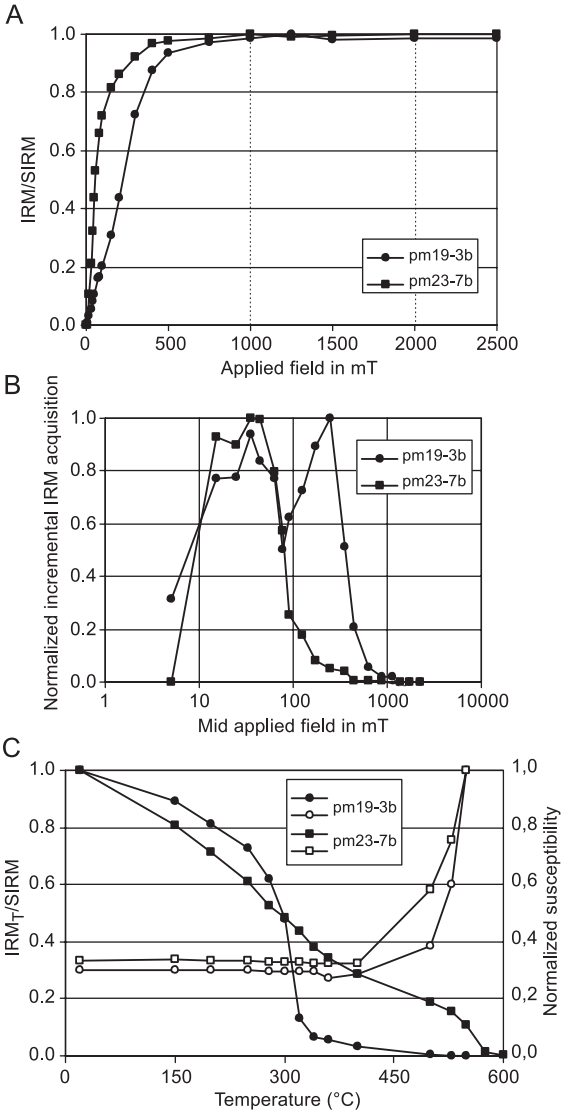

Fig. 3. (A) Isothermal remanence (IRM) acquisition curves for characteristic samples. (B) The normalized incremental IRM acquisition as a function of the applied field. (C) IRM thermal demagnetization (solid symbols) and susceptibility after heating steps (open symbols).

magnetic mineralogy. The furnaces and the SQUID magnetometer were operating in a tri-axial Helmholtz coil system maintaining an ambient field of about 10 nT in its center. This reduces the possibility of viscous remanence acquisition between heating and subsequent magnetization measurement. After each ThD step, the bulk susceptibility was measured in order to detect possible alteration upon heating.

The data set obtained by demagnetization was analysed using the PALMAG palaeomagnetic program, developed in-house at the University of Munich. This includes standard tools for processing, display and analysis of palaeomagnetic data, including principal component analysis (PCA, Kirschvink, 1980) and remagnetization circle analysis following the algorithm of McFadden and McElhinny (1988).

4. Magnetic mineralogy and remanence directions

4.1. Magnetic mineralogy

The rock magnetic data presented hereafter show that the remanence is carried mainly by magnetite and pyrrhotite. Goethite is present only in a few specimens. Hematite was not observed. No significant

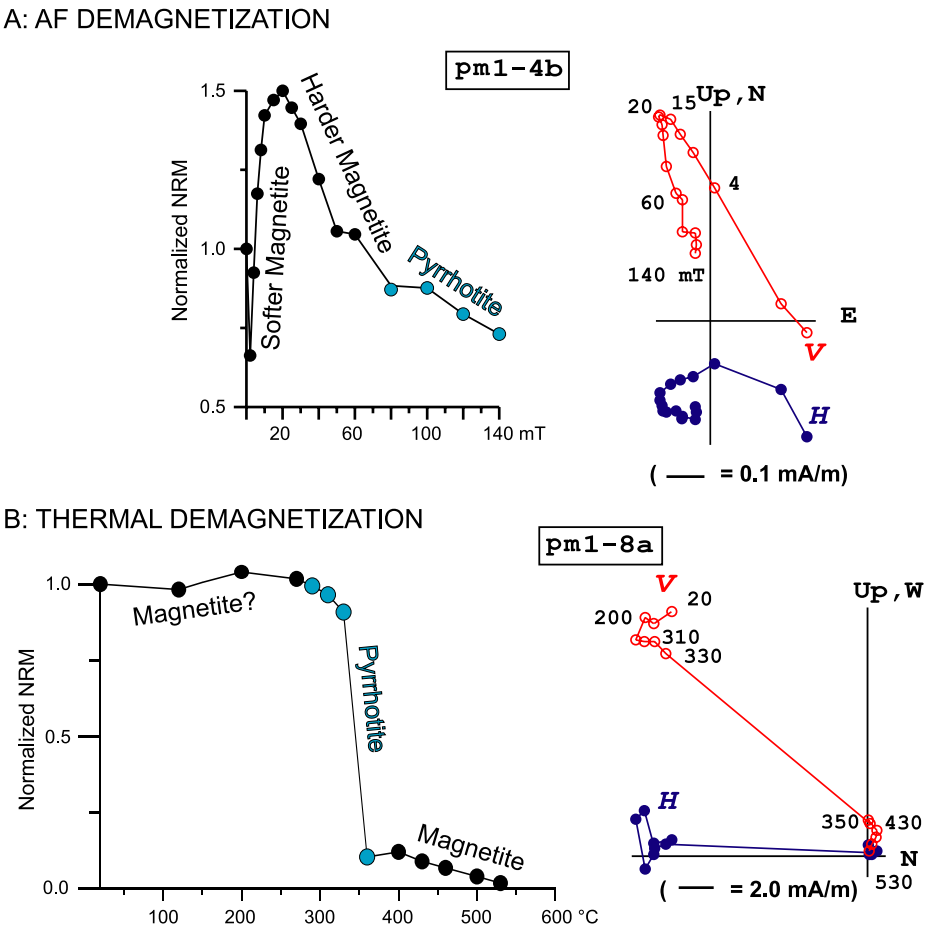

Fig. 4. Orthogonal vector projection and intensity versus stepwise demagnetization of the natural remanent magnetization (NRM) of representative specimens. (A) AF demagnetization showing three distinct components (0–20, 20–100 and >100 mT). (B) Example of thermal demagnetization evidencing three different components (0–250, 250–335 and 335–600 °C). Solid (open) symbols = horizontal (vertical) plane projection.

difference in magnetic mineralogy exists in the two sampled formations.

IRM acquisition curves show that saturation is usually reached around 1 T (Fig. 3A). The normalised incremental IRM acquisition presents a maximum at ~ 35 mT indicating mainly a low-coercive component (e.g., pm23-7b, Fig. 3B). This indicates magnetite or a low coercivity pyrrhotite component. In several cases, a second peak or higher values occur at midfields higher than 100 mT (e.g., pm19-3b, Fig. 3B), indicating the presence of a middle coercivity magnetic phase such as pyrrhotite. At applied fields higher than 1 T, no significant magnetization acquisition occurs, indicating absence of goethite or hematite. During IRM ThD, an important remanence decrease occurs at ca. 320 °C, pointing to pyrrhotite. After heating to 360 °C, 5–35% (ca. 14% in average) of the initial magnetization remains. This magnetization is completely removed at 575–600 °C evidencing magnetite. During ThD, susceptibility starts to increase dramatically between 400 and 500 °C, indicating important changes in the magnetic mineralogy of the studied samples (Fig. 3C).

Table 1
Statistical results for the pyrrhotite component including site location and bedding attitude

Site	GPS coordinates		Bedding attitude		Mean direction							
					No. of specimens used	Geographic coordinates				Stratigraphic coordinates			
	Latitude (°N)	Longitude (°E)	Dip direction (°)	Dip (°)		D_{geo} (°)	I_{geo} (°)	k	α_{95} (°)	D_{str} (°)	I_{str} (°)	k	α_{95}
pm1	29.3420	82.9799	172	16	12	192.6	−42.0	76.9	5.0	200.4	−56.6	76.9	5.0
pm2	29.3420	82.9798	226	28	12	185.5	−45.6	25.2	8.8	152.5	−61.7	25.2	8.8
pt3	29.3517	82.9787	218	42	9	194.1	−46.0	17.1	12.8	126.1	−73.6	17.1	12.8
pt4	29.3528	82.9798	208	33	11	193.7	−37.9	28.4	8.7	175.6	−68.7	28.4	8.7
pt5	29.3561	82.9819	160	17	7	203.2	−24.4	35.2	10.3	210.5	−36.1	35.2	10.3
pm6	29.3577	82.9833	128–218	15–70	7	206.8	−30.6	12.0	18.4	214.7	−62.7	5.0	28.6
pm7	29.3577	82.9833	110	15	9	198.5	−24.1	22.5	11.1	205.2	−23.6	22.5	11.1
pm8	29.4247	82.9410	40	35	8	190.2	−15.4	19.3	12.9	190.2	15.2	19.3	12.9
pm9	29.4243	82.9403	40	55	8	188.6	−24.3	10.4	18.0	188.8	23.7	10.4	18.0
pm10	29.4231	82.9383	351	32	8	215.0	−18.8	12.4	16.6	212.3	5.0	12.4	16.6
pm11	*29.4302*	*82.9212*	*225–245*	*33–40*	*3*	*247.7*	*−54.0*	*6.5*	*52.7*	*133.3*	*−6.9*	*3.1*	*86.4*
pt12	29.3995	82.9512	52	22	8	218.2	−23.7	19.1	13.0	219.4	−2.3	19.1	13.0
pt13	29.3974	82.9531	212	19	5	180.3	−30.3	37.6	12.6	171.5	−45.7	37.6	12.6
pm14	29.3979	82.9547	45	26	10	191.2	−20.7	80.9	5.4	193.6	1.3	80.9	5.4
pt15	*29.3904*	*82.9628*	*50*	*20*	*7*	*162.8*	*−4.1*	*3.7*	*29.1*	*162.1*	*3.5*	*3.7*	*29.1*
pm16	*29.3973*	*82.9708*	*18*	*24*	*7*	*192.4*	*−33.3*	*8.5*	*22.0*	*193.3*	*−9.4*	*8.5*	*22.0*
pm17	29.3963	82.9743	36	28	8	197.9	−28.9	26.7	10.9	200.2	−2.1	26.7	10.9
pm18	29.3982	82.9797	354	43	9	191.9	−24.9	15.0	13.7	190.9	16.3	15.0	13.7
pm19	29.3806	82.9870	24	47	11	179.8	−43.6	10.4	14.9	186.7	0.7	10.4	14.9
pt20	29.3817	82.9727	130	22	11	192.1	−22.3	38.3	7.5	202.4	−30.9	38.3	7.5
pm21	29.3767	82.9732	102	13	8	186.2	−28.8	11.3	17.2	193.5	−29.3	11.3	17.2
pt22	29.3655	82.9830	52	32	9	174.4	−27.8	22.7	11.0	183.0	−8.3	22.7	11.0
pm23	29.3602	82.9797	185	34	11	196.6	−20.8	10.2	15.0	203.5	−53.8	10.2	15.0
pm24	29.3472	82.9618	6	74	11	186.5	−24.1	31.9	8.2	186.7	49.9	31.9	8.2
pm25	29.3433	82.9657	215	50	10	165.9	−42.6	34.6	8.3	104.4	−53.5	34.6	8.3
pm26	29.3318	82.9633	220	17	11	161.6	−48.0	39.6	7.3	141.7	−54.4	39.6	7.3
Mean direction and statistics: $n=23$ sites ($k>10$)						191.7	−30.9	29.5	5.7	191.1	−24.4	4.3	16.6

D: declination, I: inclination, k: precision parameter, α_{95}: 95% confidence angle. Sites with low accuracy ($k<10$; $N<3$) are in italics.

NRM demagnetization usually reveals three distinct magnetic components (Fig. 4), corresponding in AFD curves (Fig. 4A) to coercivities of 2–25, 25–50 and 50–140 mT, and in ThD curves (Fig. 4B) to unblocking temperature (T_{ub}) ranges of 20– ~ 250 °C, ~ 250–335 °C and >335 °C to 500–580 °C. For many sites, the low T_{ub} (<250 °C) and the low coercivity range (<25 mT) indicate the same component with a direction in geographic coordinates ($D=354.7°$, $I=40.3°$, $\alpha_{95}=17.5°$, $N=23$) that is probably of very recent origin (present dipole field: $D/I=0°/48°$; IGRF: 0°/43°) and without palaeomagnetic significance. It can be attributed to low coercivity magnetite grains.

The other two components, demagnetized at 25–50 mT or between 475 and 580 °C and >50 mT or between 225 and 335 °C, can be related to magnetite and pyrrhotite, respectively (Fig. 4). Thermal demagnetization of NRM and IRM shows that the contribution of both components is variable (Figs. 3 and 4). For example, the pyrrhotite component is dominant in sample pm1-8a, while in sample pm1-4b, the contribution of magnetite is significantly higher than pyrrhotite.

Significant increases in susceptibility occur above 400 °C, but in most samples, no indication for a laboratory-induced remanence is observed. In some cases, viscous noise after temperature steps above

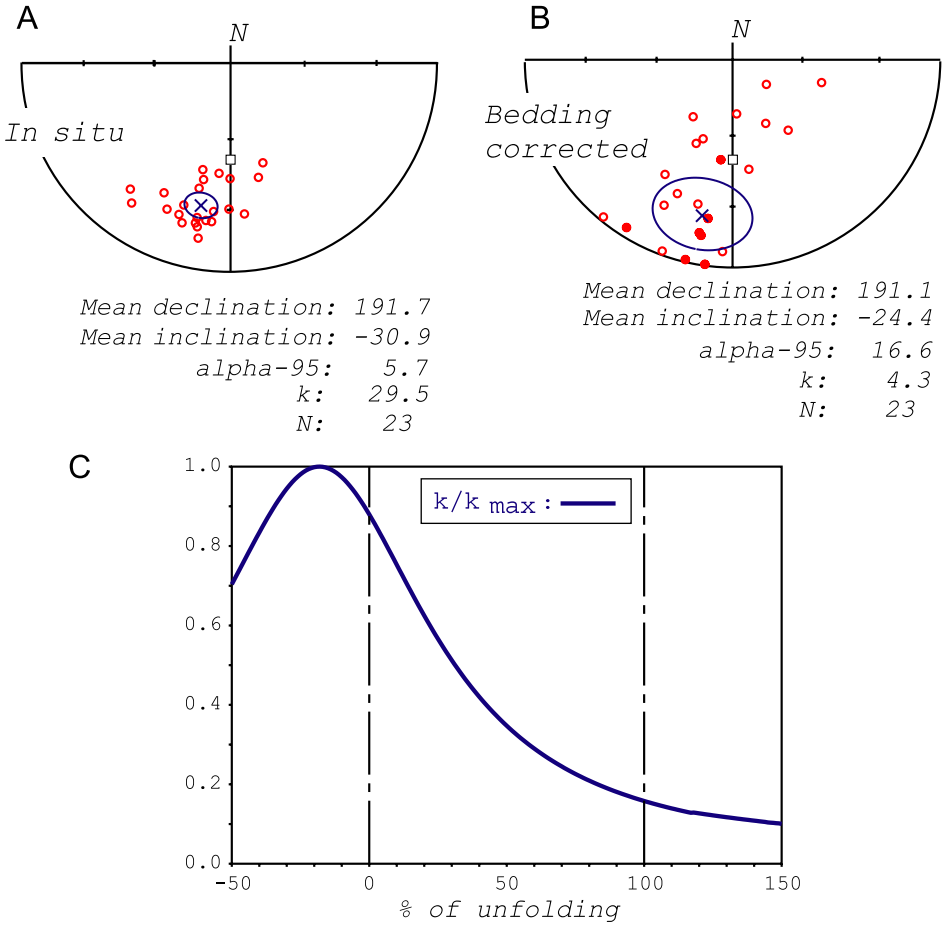

Fig. 5. Stereographic projection of the pyrrhotite site mean directions. The overall mean direction is indicated. Open (solid) circles are projected in the upper (lower) hemisphere. (A) In situ. (B) Bedding corrected. In both, the present-day dipole field reversed direction is indicated by an open square. (C) Statistical results from stepwise unfolding.

450–500 °C makes the determination of the magnetite component difficult. There is some overlap in the coercivity spectra of the pyrrhotite and magnetite components described above, but no apparent overlap between the T_{ub} ranges is observed. Both methods (AF demagnetization and ThD) were used for the assessment of the various components. Stable remanence directions were obtained for both pyrrhotite and magnetite components throughout the sample collection. Site mean directions and statistical parameters are listed in Tables 1 and 2 for the pyrrhotite and magnetite components respectively.

4.2. Pyrrhotite component

Directions characterized by intermediate T_{ub} and high coercivity reside in pyrrhotite. This is well known from many studies in other areas of the TH (Appel et al., 1991; Crouzet et al., 2001b; Schill et al., 2001, 2002a,b). The directions at site level are shown in Fig. 5. All individual specimens reveal a reverse polarity. The site mean directions with $k>10$ from 23 sites are included in the statistics (Fig. 5; Table 1). A better grouping of the site mean directions before tectonic correction is observed ($k_{in\ situ}/k_{bed.}=6.9$; Fig. 5). An incremental fold test indicates maximum grouping at −17% of unfolding implying a secondary origin of the pyrrhotite component. The in situ mean direction ($D=191.7°$, $I=-30.9°$, $\alpha_{95}=5.7°$, $k=29.5$) is significantly different from the present-day field (Fig. 6).

The inclination of the secondary pyrrhotite component from western Dolpo is shallower than that from the Hidden Valley (Crouzet et al., 2001b), Manang (Appel et al., 1991), Thakkhola ("recent component" of reverse polarity from Klootwijk and Bingham, 1980), Nar-Phu (Schill et al., 2003) and Larkya (Schill et al., submitted for publication). On the contrary, similar inclination values have been reported for the Shiar Khola (Schill et al., 2002a) and Malari (Schill et al., 2002b) areas (see Fig. 1 for approximate location of the cited areas).

4.3. Magnetite component

Directions characterized by high T_{ub} and intermediate coercivity reside in magnetite. Site mean directions are listed in Table 2. Due to the acquisition of

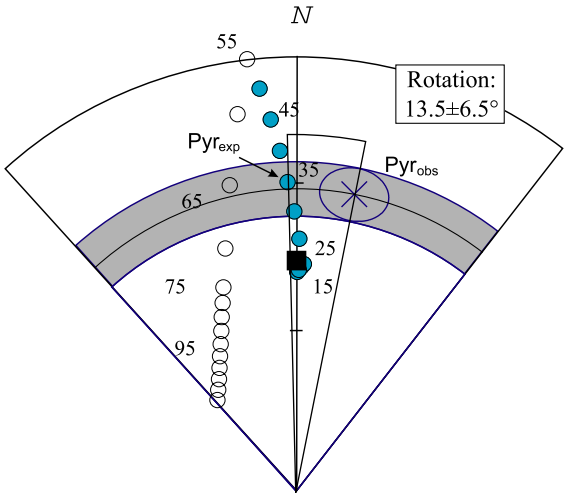

Fig. 6. Comparison of the overall pyrrhotite mean direction (cross: plotted as a normal component in the lower hemisphere) to the expected direction for an undeformed India (solid (open) circles are plotted in lower (upper) hemisphere) since Cretaceous calculated from the APWP of Acton (1999). The present-day dipole field direction is indicated by a solid square. A clockwise rotation of 13.5 ± 6.5° is deduced for a remanence age of 35 Ma.

spurious magnetization above ~450–500 °C owing to the production of a magnetic phase in several specimens, estimation of stable end-points or judgement about stability was sometimes difficult. In such cases, the mean direction was calculated by combining the remagnetization circles with stable end-points. The site mean directions from 12 sites, with $k>10$ and with a number of samples >3, are included in the statistics (Table 2). After bedding correction, the two sampled formations have very similar paleomagnetic directions: Mukut: $D=309.6°$, $I=-74.9°$, $\alpha_{95}=16.9°$, $k=9.1$, $N=10$; Tamba–Kurkur: $D=297.7°$, $I=-65.5°$, $\alpha_{95}=30.8°$, $k=68$, $N=2$. The low number of sites and the statistical parameters from the Tamba–Kurkur Formation does not allow any accurate discussion. Therefore, the overall mean direction is preferred. The mean direction of site pm19, estimated using great circles only, is not included for calculating the overall mean direction (in situ: $D=339.1°$, $I=-63.0°$, $\alpha_{95}=18.9°$, $k=6.8$, $N=11$; bedding corrected: $D=319.8°$, $I=-71.0°$, $\alpha_{95}=10.5°$, $k=19.9$, $N=11$).

The magnetite component has a northwest-oriented declination and a steep negative inclination (Fig. 7). The fold test performed using this component indi-

Table 2
Statistical results for the magnetite component

Site	Mean direction								
	No. of specimens used	Geographic coordinates				Stratigraphic coordinates			
		D_{geo} (°)	I_{geo} (°)	k	α_{95} (°)	D_{str} (°)	I_{str} (°)	k	α_{95}
pm1	10	327.5	− 64.8	26.5	9.6	336.1	− 49.7	26.5	9.6
pm2	9	308.9	− 55.9	15.5	13.7	346.5	− 49.8	15.5	13.7
pt3	6	255.7	− 44.0	23.3	16.7	313.4	− 63.8	23.3	16.7
pt4	*3*	*338.4*	*− 14.1*	*33.6*	*19.5*	*339.8*	*7.9*	*33.6*	*19.5*
pt5	*3*	*22.3*	*− 3.0*	*514.0*	*9.0*	*23.0*	*9.5*	*514.0*	*9.0*
pm6	9	180.2	32.9	12.0	15.5	181.1	− 0.2	9.3	17.9
pm7	*6*	*133.3*	*55.4*	*6.9*	*28.3*	*127.4*	*41.3*	*6.9*	*28.3*
pm8	low amount of magnetite								
pm9	8	216.2	47.4	33.1	10.2	51.8	77.3	33.1	10.2
pm10	*11*	*321.9*	*− 64.2*	*6.9*	*18.9*	*224.9*	*− 74.8*	*6.9*	*18.9*
pm11	low amount of magnetite								
pt12	*3*	*217.3*	*− 38.7*	*68.5*	*24.9*	*220*	*− 17.3*	*68.5*	*24.9*
pt13	low amount of magnetite								
pm14	low amount of magnetite								
pt15	low amount of magnetite								
pm16	10	335.4	− 47.1	41.9	8.1	307.1	− 60.8	41.9	8.1
pm17	11	355.6	− 61.7	31.5	8.8	288.9	− 71.2	31.5	8.8
pm18	8	3.8	− 50.2	18.3	14.8	113.9	− 82.8	18.3	14.8
pm19	8	203.5	− 83.1	144.3	5.4	203.9	− 36.1	144.3	5.4
pt20	4	217.6	− 78.4	154.6	14.3	280.8	− 65.7	154.6	14.3
pm21	7	60.6	− 66.7	36.5	11.6	29.5	− 74.1	36.5	11.6
pt22	low amount of magnetite								
pm23	low amount of magnetite								
pm24	7	352.1	− 9.0	43.7	11.2	301.6	− 74.7	43.7	11.2
pm25	low amount of magnetite								
pm26	5	299.3	− 63.2	25.7	19.1	332.2	− 61.4	25.7	19.1
Mean direction:									
12 Sites ($k>10$, $N>3$)		337.9	− 65.9	6.8	17.9	306.5	− 73.3	10.7	13.9
11 Sites (excluding pm19)		339.1	− 63.0	6.8	18.9	319.8	− 71.0	19.9	10.5

For legend, see Table 1.

cates a best grouping at ~ 75% ($D=326.5°$; $I=-69.7°$; $\alpha_{95}=9.2°$; $k=25.5$) of unfolding. According to this result, the magnetization should have been acquired during the deformation, i.e., during Tertiary. If we accept a Tertiary age for the remanence, it implies that (1) the palaeogeographic location of the studied area was in the southern hemisphere during Tertiary, or (2) large rotation (>100°) around a vertical axis in case of a reverse polarity component, or large tilting (~ 80°) around horizontal axis in case of a normal polarity component, occurred since remanence acquisition. Such scenarios are geologically unrealistic, and the difference in statistic parameters between the best grouping at 75% ($\alpha_{95}=9.2°$; $k=25.5$) and at 100% ($\alpha_{95}=10.5°$; $k=19.9$) of unfolding are not so different to exclude a

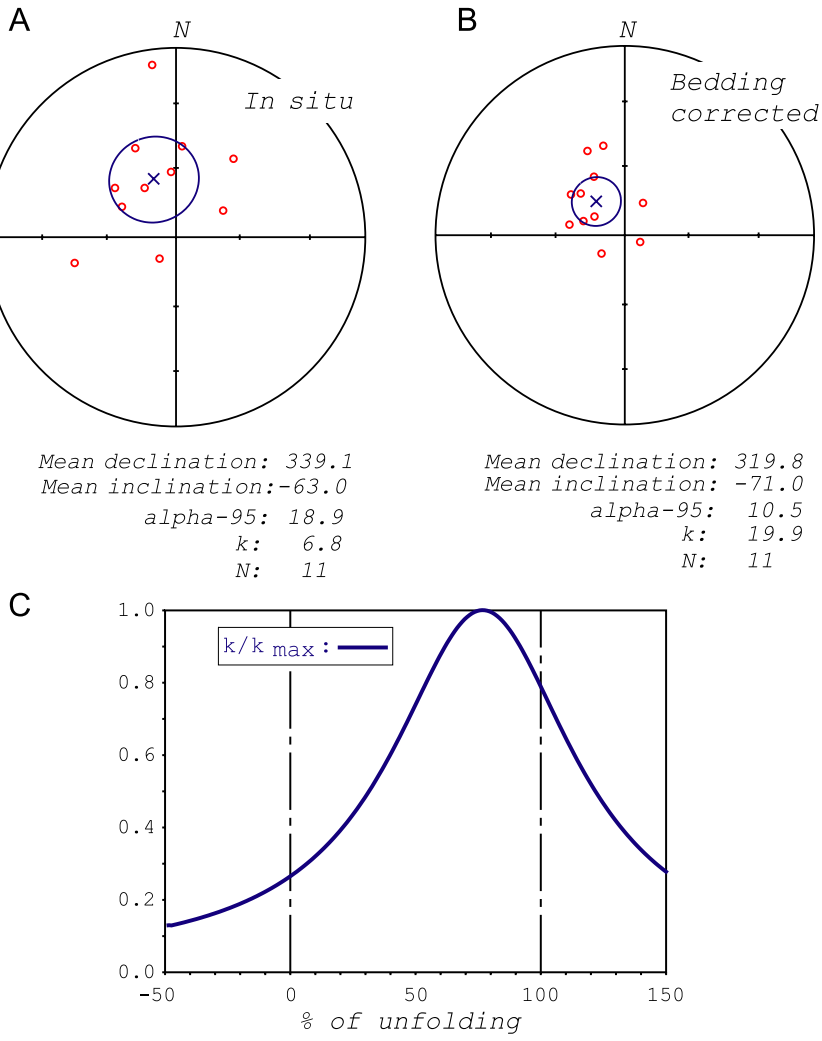

Fig. 7. Stereographic projection (upper hemisphere) of the magnetite site mean directions. The overall mean direction is indicated. (A) In situ. (B) Bedding corrected. (C) Statistical results from stepwise unfolding. Notice that pm9 (originally reverse polarity) is plotted here as a normal polarity direction.

prefolding age for the remanence. The age of the Mukut and the Tamba–Kurkur Formations is about ~ 250–220 Ma (Griesbachian to early Lacian). The observed overall mean direction after complete bedding correction ($D/I = 319.8°/-71.0°$) is close to the expected direction for a Triassic primary direction (at 220 Ma: $D_{exp} = 303.1°$, $I_{exp} = -54.8°$; at 250 Ma: $D_{exp} = 306.3°$, $I_{exp} = -68.0°$) calculated from the APWP for Gondwana of Van der Voo (1993) rotated to the Indian plate using the Euler pole and rotation angle provided by Scotese and McKerrow (1991). Therefore, the magnetite component described in this paper may reside in a DRM or in a CRM acquired during the first stage of diagenesis as it was demonstrated in the French Vocontian trough (Katz et al., 2000). The sites have predominantly a reverse polarity, but the occurrence of one site with normal polarity (pm9) suggests the magnetization to be of sedimentary origin. The inclination for the magnetite component from Dolpo is steeper than the Triassic primary components reported from adjacent areas (Thakkhola: $D = 323°$ to $329°/I = -43°$ to $-48°$, Klootwijk and

Bingham, 1980; Manang: $D=334°/I=-54°$, Appel et al., 1991; Shiar Khola: $D=6.9°/I=-63.7°$, Schill et al., 2002a).

5. Discussion and conclusion

5.1. Origin of pyrrhotite

It is generally accepted that in low metamorphic marly carbonates, pyrrhotite is formed at elevated temperature (anchimetamorphism to greenschist facies) by the breakdown of primary magnetite and/or pyrite. The occurrence of sulphides in metamorphic rocks suggests low oxygen fugacity implying that sedimentary (detrital and/or authigenic) pyrite may also have been reduced into pyrrhotite during low-grade prograde metamorphism (Carpenter, 1974; Ferry, 1981; Mohr and Newton, 1983; Hall, 1986; Tracy and Robinson, 1988). Transformation of magnetite into pyrrhotite is widely reported from the western Alps (Rochette and Lamarche, 1986; Rochette, 1987). According to Crerar et al. (1978), this transformation may start if there is either a decrease in oxygen fugacity or an increase in sulphur fugacity. The occurrence of both magnetite and pyrrhotite in the studied area is an indication for this transformation. Both minerals can easily coexist if the reactions are not complete.

5.2. Nature of remanences

The negative fold test for the pyrrhotite directions implies a secondary origin of pyrrhotite magnetization (Fig. 5). Under metamorphic conditions, grains with blocking temperature (T_b) higher than the temperature reached during metamorphism (T_m) will acquire a CRM during grain growth, while grains with $T_b<T_m$ will acquire a TRM during cooling. Therefore, in a metamorphic rock (assemblage of different grain sizes), where it cannot be demonstrated that $T_m>T_{curie}$, the remanence acquired may be best described as a thermochemical remanent magnetization (TCRM). In western Dolpo, the maximum temperature reached was never higher than ~275–300 °C based on vitrinite reflectance and illite crystallinity studies (Garzanti et al., 1994; Crouzet et al., 2002b) and the pyrrhotite remanence has a single reverse polarity characterized by a T_{ub} range of 270–335 °C. Therefore, a TCRM origin is most probable.

The magnetite direction is consistent with other Triassic primary directions from TH (Klootwijk and Bingham, 1980; Appel et al., 1991; Schill et al., 2002a) although it is slightly steeper. Comparison of the measured inclination with the expected one is illustrated in Fig. 8. The measured mean inclination is in good agreement with the expected one for an age of ~250–220 Ma. Therefore, we believe that the magnetite remanence is a primary one acquired during sedimentation or during the first stages of diagenesis in Triassic times. Using different APWPs does not change the principal results. However, the 95% confidence limits are wide and imply a wide range of age uncertainties.

5.3. Age of pyrrhotite magnetization

The age of the secondary pyrrhotite remanence can be determined by different approaches: (1) using geochronological data on the age of low-grade metamorphism during which pyrrhotite is assumed to be formed; and (2) using inclination matching, i.e., through comparison of the measured inclination with the expected one for different ages.

K/Ar ages reported in the studied area by Crouzet et al. (2002b) are not reset, and, therefore, they are not representative for the age of metamorphism. No other geochronological data exist for this part of the Himalayan belt. However, Crouzet et al. (2002b) report a general trend of low-grade metamorphic ages, mainly based on K/Ar illite or white micas dating, decreasing from Zanskar (45–47 Ma) to central Nepal (25–30 Ma). Assuming the validity of this trend, it is possible to estimate the age of low-grade metamorphism in western Dolpo at around 32 ± 2 Ma.

Inclination matching is very uncertain because several complications may have occurred since the time of magnetization: (i) possible huge amount of N–S shortening along major thrusts, in respect to the Indian plate, (ii) regional scale tilting such as MCT ramping (Appel et al., 1991; Rochette et al., 1994; Crouzet et al., 2001b) or long-wavelength folding (Schill et al., 2002a) and (iii) local rotations postdating the pyrrhotite remagnetization along the

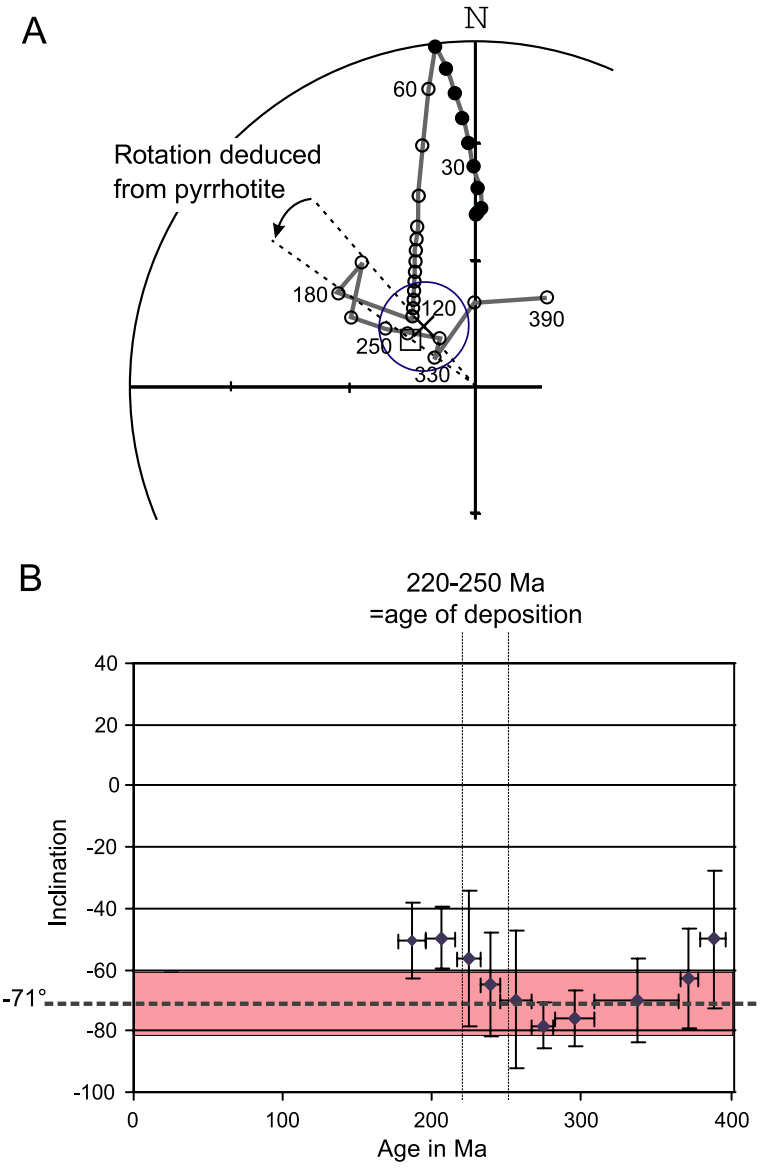

Fig. 8. (A) Comparison of the magnetite overall mean direction and the expected direction, calculated up to 120 Ma from the APWP of Acton (1999) and for earlier periods from the Gondwana APWP (Van der Voo, 1993) rotated to the Indian plate using Euler poles of Scotese and McKerrow (1991). Ages are given in Ma. Cross: magnetite mean direction. Square: magnetite direction after correction based on the rotation deduced from the pyrrhotite component. Open (close) circles: expected directions in the upper (lower) hemisphere. (B) Expected inclination calculated from Van der Voo (1993) versus age. Magnetite inclination measured in Dolpo (dashed line) and its uncertainty (grey area) are indicated.

TH in the Zanskar and Shiar areas (Schill et al., 2001, 2002a). Ignoring such complications, the test illustrated in Fig. 9 indicates a possible age of magnetization at around 34.0 $+7.9/-9.0$ Ma using graphical determination of inclination matching. This is surprisingly similar to the age deduced from the general E–W trend of geochronological data.

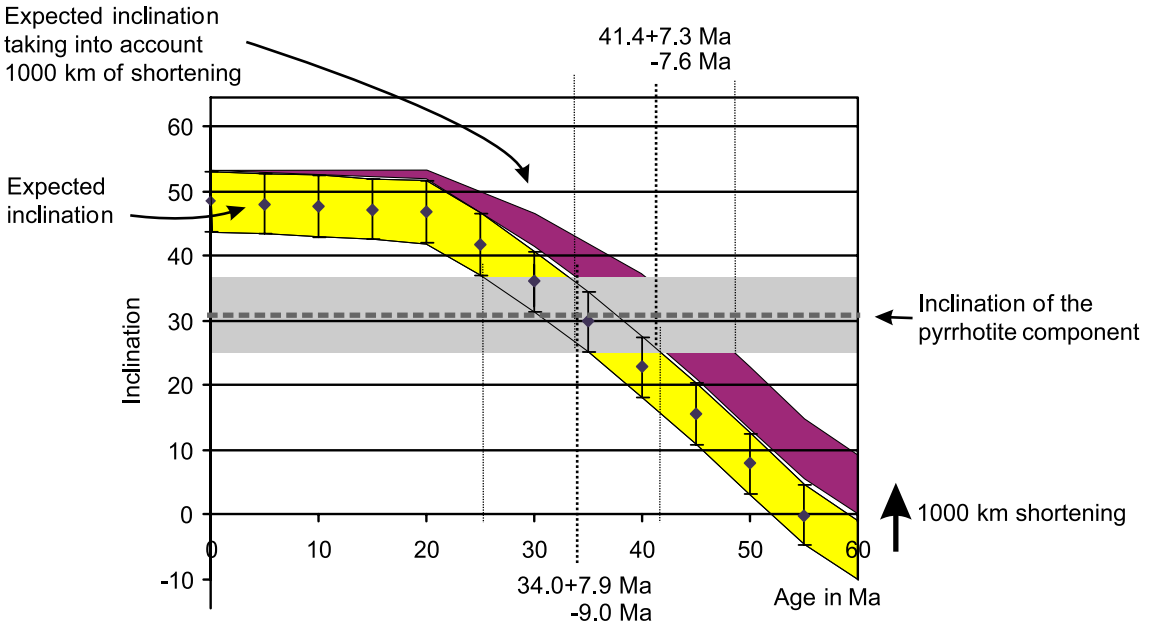

Fig. 9. Pyrrhotite inclination matching with the Indian APWP (Acton, 1999). The effect of a crustal shortening of 1000 km is illustrated. See text for further discussion.

From the northward movement of Indian subcontinent (Dewey et al., 1989; Le Pichon et al., 1992) and southern Tibet (Besse and Courtillot, 1988) since the time of collision, a shortening between stable India and South Tibet of about 600 ± 900 km can be calculated. Also, higher values, as much as 1000–1500 km, have been proposed (Chen et al., 1993; Patzelt et al., 1996). Taking into account 1000 km of crustal shortening between the Dolpo area and stable India since remanence acquisition, the inclination matching provides a possible age of $41.4\ ^{+7.3}_{-7.6}$ Ma (Fig. 9). These values are only slightly older that the age estimated from geochronological data.

Finally, we conclude that an age of ~ 35 Ma can be estimated for the pyrrhotite remanence.

5.4. Discussion on rotations

Using 35 Ma as the age of pyrrhotite magnetization acquisition, a significant clockwise rotation of $13.5 \pm 6.5^\circ$ versus the Indian plate is demonstrated, by comparison with the APWP of Acton (1999) (Fig. 6). Several types of rotation have been reported in the Himalayan belt by palaeomagnetists over the last 20 years. Deviation of observed declinations from the expected one (calculated from the APWP based on an undeformed Indian continent with the present day geometry) has been interpreted in terms of (1) rotational underthrusting, (2) oroclinal bending and (3) local to mesoscale rotations.

1. Rotational underthrusting of India beneath its northern margin and Asia is expected as a consequence of the counterclockwise rotation of India. It can be regarded as a uniform counterclockwise movement of the Indian shield around a pivot in the western syntaxis (35°N/73°E; Klootwijk et al., 1985). Therefore, declination measured in the TH should exhibit a clockwise rotation when compared with the expected one from stable India. This is compatible with the $13.5 \pm 6.5^\circ$ rotation reported in this paper.
2. Oroclinal bending can be described by block rotations around several pivots along a small circle following the Himalayan arc (Klootwijk et al., 1985). Its driving mechanism is assumed to be the underthrusting of the Indian lithosphere along major crustal thrusts (Treloar and Coward, 1991). Rotation due to oroclinal bending for the Dolpo

Table 3
Pyrrhotite directions and poles

Location			Pyrrhotite (geographic coordinates)					Pyrrhotite South Pole		Expected South Pole		Rotation pole		
Region	Latitude	Longitude	D	I	α_{95}	k	Age in Ma	Lat.	Long.	Lat.	Long.	Long.	Lat.	Angle
Western Dolpo	29.3779	82.9669	191.7	−30.9	5.7	29.5	35	−73.4	40.3	−76.5	90.2	78.4	13.2	12.9
Thakkhola	28.7000	83.7000	184.4	−54.3	12.2	31.0	30	−82.8	294.0	−80.6	86.4	8.3	2.0	16.1
Manang	28.6700	84.0000	196.4	−65.9	3.2	183.0	30	−66.7	292.5	−80.6	86.4	15.3	3.1	32.0
Shiar	28.6000	85.1000	206.9	−27.2	6.8	15.2	25	−61.3	19.1	−84.6	77.7	99.9	5.0	26.2

The rotations deduced from the comparison between the poles calculated from the pyrrhotite component and the APWP of Acton (1999) are indicated. Measured directions are from Klootwijk and Bingham (1980) for the Thakkhola area, Appel et al. (1991) for the Manang area and Schill et al. (2002a) for the Shiar area. See Table 1 for legend. Lat.: latitude, Long.: longitude.

area can be estimated taking into account the small-circle geometry around the Turfan pole (42.5°N, 91.1°E) defined by Klootwijk et al. (1985) and assuming a zero rotation on the bisector of the small circle between the western and eastern syntaxes of the Himalayan arc. This estimation yields a 5–10° clockwise rotation relative to stable India, compatible with the results in this study.

3. Local rotations are observed, even within a few tens of kilometers, as it was shown, for example, by Appel et al. (1995) for NW Zanskar and by Schill et al. (2001) in SE Zanskar. Close to major tectonic features, local rotations completely dominate, e.g., along the Indus–Yarlung Suture (Otofuji et al., 1989), and within the Pamir Range (Waldhör et al., 2001).

According to Acton's (1999) APWP, the counter-clockwise rotation of the Indian plate since 35–40 Ma is not more than 5°. The $13.5 \pm 6.5°$ clockwise rotation evidenced by the pyrrhotite ChRM may be decomposed into 5° due to rotational underthrusting plus 5–10° due to oroclinal bending. Rotational underthrusting was also evidenced by back rotating the effects of regional scale and oroclinal bending rotations in NW Himalaya (Schill et al., 2001). We cannot exclude that the rotation evidenced in this paper is also completely or partly due to local effects.

Different block rotations on local to regional scales lead to errors in the estimated amount of rotational shortening and/or oroclinal bending caused by the rotation of India. The palaeomagnetic significance of the oroclinal bending and rotational underthrusting model strongly depends on the regional significance of declination anomalies. The data set presented in this study, even when considered together with the previously published results, is still not sufficient to allow quantitative modelling.

The rotation evidenced by pyrrhotite obviously postdates the magnetite remanence. Therefore, the latter was rotated around a vertical axis by the amount

Table 4
Magnetite palaeomagnetic directions and associated poles (before and after rotation correction deduced from the secondary pyrrhotite directions) for the Dolpo (this study), Thakkhola (Klootwijk and Bingham, 1980), Manang (Appel et al., 1991) and Shiar (Schill et al., 2002a) areas

Region	Magnetite (bedding corrected)				South Pole				Pole corrected according to pyrrhotite data			
	D	I	α_{95}	k	Lat.	Long.	A_{95}	K	Lat.	Long.	A_{95}	K
Western Dolpo	319.8	−71.0	10.5	19.9	1.5	104.5			7.3	106.6		
Thakkhola	325.5	−46.0	5.2	565.8	−24.9	117.4			−9.6	116.3		
Manang	334.3	−54.1	4.2	30.2	−22.2	106.7			9.7	108.3		
Shiar	6.9	−63.7	10.8	11.0	−15.8	80.1			−22.3	91.3		
Mean	335.8	−59.8	17.0	30.2	−15.8	102.0	22.2	18.1	−3.7	105.9	21.1	20.0
Mean, excluding Shiar	327.6	−57.1	20.4	37.4	−15.3	109.3	24.7	26.0	2.5	110.4	18.0	48.0

D: declination, I: inclination, k: precision parameter, α_{95}: 95% confidence angle, Lat.: latitude, Long.: longitude, A_{95}: 95% confidence angle of the pole, K: precision parameter of the pole.

of the rotation deduced from the pyrrhotite component, to its original position ($D=306.3°$, $I=-71.0°$). Combining the uncertainty on the pyrrhotite rotation ($\pm 6.5°$) and the α_{95} of the measured magnetite direction after bedding correction leads after Demarest (1983) to a new confidence limit at 9.9° for the mean direction. Comparing the resulting magnetite direction to the expected direction according to the APWP indicates no significant rotation of the studied area versus stable India between Triassic and Middle/Upper Eocene. Notice that this conclusion is only tentative because of the steep inclination of magnetite component and the large uncertainty in declination (rotation).

In order to test the conclusion reached above, other prefolding magnetite directions from the TH in the central part of the Himalayan belt have been taken into account. Magnetite components from the Manang (Appel et al., 1991) and Thakkhola areas (Klootwijk and Bingham, 1980) have directions similar to the Dolpo results. In a lesser degree, this is also valid for the Shiar Khola area (Schill et al., 2002a). In the Manang and Thakkhola areas, the pyrrhotite component is steeper than the present-day dipole field inclination indicating late tilting (Table 3). Also, the declination shows significant deviation from the expected one. The magnetite directions can be corrected for the deformation postdating the pyrrhotite remanence. We prefer to use only a single rotation around an inclined axis. Note that this deformation is probably a combination of a rotation around a vertical axis, as evidenced for the Dolpo area, and a rotation around a horizontal axis. However, the chronology of both deformations is unknown. The axis and the angle of rotation are deduced from the comparison between the pole calculated using the pyrrhotite component and the expected pole according to Acton (1999) assuming a magnetization age compatible with the general E–W trend in geochronological data. Using this result, the geomagnetic poles calculated from the bedding-corrected magnetite directions for the different areas are corrected in order to calculate their positions before the time of pyrrhotite remanence acquisition (Table 4). Combining magnetite poles from the different areas (Table 4) gives a mean south pole position of Lat $=-3.7°$, Long $=105.9°$, $A_{95}=21.1°$ and $K=20$. This correction does not improve significantly the grouping (before correction: $A_{95}=22.2°$ and $K=18.1$). In the Shiar area, a late folding, scattering the pyrrhotite directions along a small circle, has been described (Schill et al., 2002a). Also, the magnetite direction for the Shiar area is different from the other ones. Excluding Shiar, results in a significantly improved pole mean direction after correction (Lat $=2.5°$, Long $=110.4°$, $A_{95}=18°$, $K=48$). Therefore, it is suggested that magnetite components were dispersed after pyrrhotite remanence acquisition. Comparing this mean value to the APWP (Fig. 10) shows that the calculated rotation, versus stable India, is minimum at ~ 250 Ma. This is in very good agreement with the expected Triassic age for the magnetite remanence.

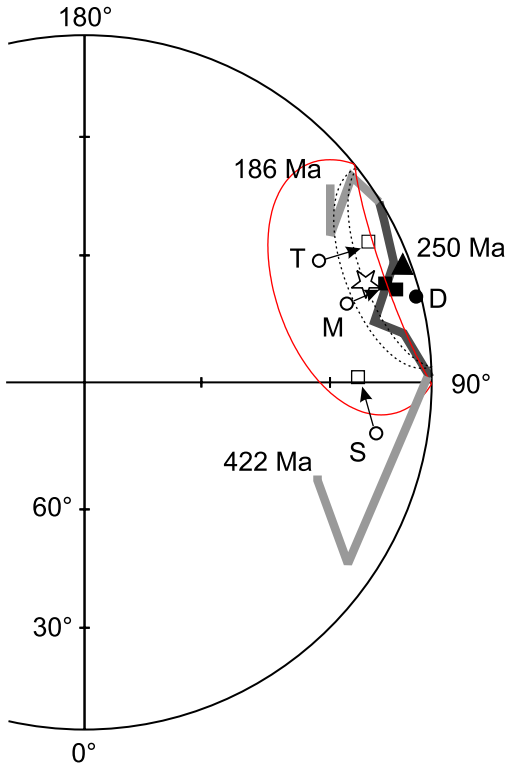

Fig. 10. Stereoplot of the poles deduced from magnetite components before (circles) and after pyrrhotite correction (squares) from different areas: T—Thakkhola, D—Dolpo, S—Shiar, M—Manang. The mean directions and confidence circle before (star, solid line) and after (triangle, dashed line) correction are calculated using only T, D and M data. Open (solid) symbols are plotted in upper (lower) hemisphere. The APWP (Van der Voo, 1993) is also indicated (light grey: upper hemisphere, dark grey: lower hemisphere). For further discussion, see text.

5.5. Tectonometamorphic consequences

Assuming a Triassic age for the magnetite component implies that no important rotations have occurred in TH between Triassic and late Eocene (the age of the pyrrhotite remanence acquisition). As collision did not occur before 55 Ma, the possible age of folding is restricted between 55 and 35 Ma. The pyrrhotite formation occurred probably during metamorphism between 40 and 35 Ma. This is compatible with an Eo-Himalayan metamorphism (M1). Occurrence of only one pyrrhotite component suggests that the Neo-Himalayan metamorphic phase (M2), which is predominant in the HHC, did not affect significantly the western Dolpo area.

Acknowledgements

We thank C.T. Klootwijk and an anonymous reviewer for constructive comments and corrections, and G. Fuchs for help during the preparation of fieldwork. L. Paudel, K. Regmi and M. Staiger took part in discussions on various aspects. Participation of R. Schuster during sampling in Dolpo and his comments on the regional geology is acknowledged. The German Research Council (DFG) funded this study within project AP 34/9.

References

Acton, G.D., 1999. Apparent polar wander of India since the Cretaceous with implications for regional tectonics and true polar wander. Mem. Geol. Soc. India 44, 129–175.

Appel, E., Müller, R., Widder, R.W., 1991. Palaeomagnetic results from the Tibetan sedimentary series of the Manang area (north central Nepal). Geophys. J. Int. 104, 255–266.

Appel, E., Patzelt, A., Chouker, C., 1995. Secondary palaeoremanence of Tethyan sediments from the Zanskar range (NW Himalaya). Geophys. J. Int. 122, 227–242.

Bassoulet, J.P., Boulin, J., Colchen, M., Marcoux, J., Mascle, G., Montenat, C., 1980. Evolution des domains Téthysiens au pourtour du Bouclier Indien du Carbonifère au Crétacé. Géologie des Chaînes Alpines issues de la Téthys, Colloque C5, 26th International Geological Congres, Mém. BRGM, Paris, vol. 115, 180–198.

Besse, J., Courtillot, V., 1988. Paleogeographic maps of the continents bordering the Indian Ocean since the early Jurassic. J. Geophys. Res. 93, 11791–11808.

Brookfield, M.E., 1993. The Himalayan passive margin from Precambrian to Cretaceous time. Sediment. Geol. 84, 1–35.

Carpenter, R.H., 1974. Pyrrhotite isograde in the SE Tennessee and SW North Carolina. Geol. Soc. Amer. Bull. 85, 451–456.

Chen, Y., Courtillot, V., Cogné, J.-P., 1993. The configuration of Asia prior to the collision of India: Cretaceous paleomagnetic constraints. J. Geophys. Res. 98 (B12), 21941–21972.

Colchen, M., Le Fort, P., Pêcher, A., 1980. Carte géologique Annapurna–Manaslu–Ganesh. Himalaya de Népal. Echelle 1/200.000. Ed. C.N.R.S., Science de la Terre, Paris.

Crerar, D.A., Susak, N.J., Borsik, M., Schwartz, S., 1978. Solubility of the buffer assemblage pyrite+magnetite in NaCl solutions from 200 to 350 °C. Geochim. Cosmochim. Acta 42, 1427–1437.

Crouzet, C., Paudel, L., Dunkl, I., Appel, E., Árkai, P., Balogh, K., Rainer, T.M., 2001a. New constraints on the tectono-thermal evolution of the Tethyan Himalaya (Western Nepal). J. Asian Earth Sci. 19 (3A), 10–11.

Crouzet, C., Stang, H., Appel, E., Schill, E., Gautam, P., 2001b. Detailed analysis of successive pTRMs carried by pyrrhotite in Himalayan metacarbonates: an example from Hidden Valley, Central Nepal. Geophys. J. Int. 146, 607–618.

Crouzet, C., Dunkl, I., Paudel, L., Árkai, P., Rainer, T.M., Balogh, K., Appel, E., 2002a. New geothermometrical and geochronological results from Tethyan Himalaya (Dolpo–Manang areas, Nepal). J. Asian Earth Sci. 20 (4A), 7–8.

Crouzet, C., Paudel, L., Dunkl, I., Appel, E., Árkai, P., Balogh, K., Rainer, T.M., 2002b. New constraints on the tectono-thermal evolution of the Tethyan Himalaya (Western Nepal). Abstracts for the 17th HKTW. J. Asian Earth Sci. 20 (4, Suppl. 1), 1–55.

Demarest, H., 1983. Error analysis for the determination of tectonic rotation from paleomagnetic data. J. Geophys. Res. 88, 4321–4328.

Dewey, J., Cande, S., Pitman, W., 1989. Tectonic evolution of the India/Eurasia Collision Zone. Eclogae Geol. Helv. 82 (3), 717–734.

Ferry, J.M., 1981. Petrology of graphitic sulfide-rich schists from south-central Maine: an example of desulfidation during prograde regional metamorphism. Am. Mineral. 66, 908–930.

Fuchs, G., 1967. Zum Bau des Himalaya. Osterreichische Akademie der Wissenschaften, Mathematisch-Naturwissenschaftliche Klasse Denkschriften, 113 band, Wien, 1–212.

Fuchs, G., 1977. The geology of the Karnali and Dolpo regions, western Nepal. Jahrb. Geol. Bundesanst., Wien 120, 165–217 (and map).

Fuchs, G., Widder, R.W., Tuladhar, R., 1988. Contributions to the geology of the Annapurna Range (Manang area, Nepal). Jahrb. Geol. Bundesanst., Wien 131, 593–607.

Garzanti, E., 1999. Stratigraphy and sedimentary history of the Nepal Tethys Himalaya passive margin. J. Asian Earth Sci. 17, 805–827.

Garzanti, E., Gorza, M., Martellini, L., Nicora, A., 1994. Transition from diagenesis to metamorphism in the Paleozoic to Mesozoic succession of the Dolpo–Manang Synclinorium and Thakkhola Graben (Nepal Tethys Himalaya). Eclogae Geol. Helv. 87, 613–632.

Godin, L., Brown, R., Hanmer, S., Parrish, R., 1999. Back folds in

the core of the Himalayan orogen: an alternative interpretation. Geology 27 (2), 151–154.

Godin, L., Parrish, R.R., Brown, R.L., Hodges, K.V., 2001. Crustal thickening leading to exhumation of the Himalayan Metamorphic core of central Nepal: insight from U–Pb geochronology and 40Ar/39Ar thermochronology. Tectonics 20 (5), 729–747.

Guillot, S., Cosca, M., Allemand, P., 1999. Contrasting metamorphic and geochronologic evolution along the Himalayan belt. Geol. Soc. Am. Spec. Paper 328, 117–127.

Hall, A.J., 1986. Pyrite–pyrrhotite redox reactions in nature. Mineral. Mag. 50, 223–229.

Hodges, K.V., 2000. Tectonics of the Himalaya and southern Tibet from two perspectives. Geol. Soc. Amer. Bull. 112 (3), 324–350.

Hodges, K.V., Parrish, R.R., Searle, M.P., 1996. Tectonic evolution of the central Annapurna range, Nepalese Himalayas. Tectonics 15, 1254–1291.

Katz, B., Elmore, R.D., Cogoini, M., Engel, M.H., Ferry, S., 2000. Associations between burial diagenesis of smectite, chemical remagnetization and magnetite authigenesis in the Vocontian trough, SE France. J. Geophys. Res. 105, 851–868.

Kirschvink, J.L., 1980. The least-squares line and plane and the analysis of palaeomagnetic data. Geophys. J. R. Astron. Soc. 62, 699–718.

Klootwijk, C.T., Bingham, D.K., 1980. The extent of Greater India: III. Palaeomagnetic data from the Tibetan series, Thakkhola region, Nepal Himalaya. Earth Planet. Sci. Lett. 51, 381–405.

Klootwijk, C.T., Conaghan, P., Powell, C., 1985. The Himalayan Arc: large-scale continental subduction, oroclinal bending and back-arc spreading. Earth Planet. Sci. Lett. 75, 167–183.

Klootwijk, C.T., Gee, J.S., Peirce, J.W., Smith, G.M., 1991. Constraints on the India–Asia convergence: paleomagnetic results from Ninetyeast Ridge. In: Weissel, J., Peirce, J., et al., (Eds.), Proceedings of the Ocean Drilling Program, Scientific Results, College Station, TX, Ocean Drilling Program, vol. 121, pp. 777–881.

Le Pichon, X., Fournier, M., Jolivet, L., 1992. Kinematics, topography, shortening, and extrusion in the India–Eurasia collision. Tectonics 11 (6), 1085–1098.

McFadden, P.L., McElhinny, M.W., 1988. The combined analysis of remagnetisation circles and direct observations in palaeomagnetism. Earth Planet. Sci. Lett. 87, 161–172.

Mohr, D.W., Newton, R.C., 1983. Kyanite–staurolite metamorphism in sulfidic schists of Anakeesta formation, Great Smoky Mountains, North Carolina. Am. J. Sci. 283, 135–165.

Otofuji, Y., Funahara, S., Matsuo, J., 1989. Paleomagnetic study of western Tibet: deformation of a narrow zone along the Indus Zangbo suture between India and Asia. Earth Planet. Sci. Lett. 92, 307–316.

Patzelt, A., Li, H., Wang, J., Appel, E., 1996. Palaeomagnetism of Cretaceous to tertiary sediments from southern Tibet: evidence for the extent of the northern margin of India prior to the collision with Eurasia. Tectonophysics 259, 259–284.

Rochette, P., 1987. Metamorphic control of the magnetic mineralogy of black shales in the Swiss Alps, toward the use of "magnetic isograde". Earth Planet. Sci. Lett. 84, 446–456.

Rochette, P., Lamarche, G., 1986. Evolution des propriétés magnétiques lors des transformations minérales dans les roches: exemple du Jurassique Dauphinois (Alpes françaises). Bull. Minéral. 109, 687–696.

Rochette, P., Scaillet, B., Guillot, S., Le Fort, P., Pecher, A., 1994. Magnetic properties of the high Himalayan leucogranites: structural implications. Earth Planet. Sci. Lett. 126, 214–234.

Schill, E., Appel, E., Zeh, O., Singh, V.K., Gautam, P., 2001. Coupling of late-orogenic tectonics and secondary pyrrhotite remanences: towards a separation of different rotation processes and quantification of rotational underthrusting in the western Himalayas (N-India). Tectonophysics 337, 1–21.

Schill, E., Appel, E., Gautam, P., Dietrich, P., 2002a. Thermo-tectonic history of the Tethyan Himalayas deduced from palaeomagnetic record of metacarbonates from central Nepal (Shiar Khola). J. Asian Earth Sci. 20 (3), 203–210.

Schill, E., Crouzet, C., Gautam, P., Singh, V.K., Appel, E., 2002b. Where did rotational shortening occur in the Himalayas? Inferences from palaeomagnetic analyses of remagnetisations. Earth Planet. Sci. Lett. 203, 45–57.

Schill, E., Appel, E., Godin, L., Crouzet, C., Gautam, P., Regmi, K., 2003. Record of deformation by secondary magnetic remanences and magnetic anisotrophy in the Nar/Phu valley (central Himalaya). Tectonophysics 377, 197–209, this issue.

Schill, E., Crouzet, C., Wehland, F., Gautam, P., Appel, E., Guillot, S., submitted for publication. Multi-stage deformation record of secondary pyrrhotite remanences in Larkya area (Central Nepal), Tectonics.

Schneider, C., Masch, L., 1993. The metamorphism of the Tibetan series from the Manang area, Marsyandi Valley, Central Nepal. Geol. Soc. Spec. Publ. 74, 357–374.

Scotese, C.R., McKerrow, W.S., 1991. Ordovician plate tectonic reconstructions. In: Barnes, C.R., Williams, S.H. (Eds.), Advances in Ordovician Geology. Geol. Surv. Canada, paper 90–9, pp. 271–282.

Searle, M., Windley, B., Coward, M., 1987. The closing of Tethys and the tectonics of the Himalaya. Geol. Soc. Amer. Bull. 98, 678–701.

Tracy, R.J., Robinson, P., 1988. Silicate–sulfide–oxide–fluid reactions in granulite grade pelitic rocks. Central Massachusetts. Am. J. Sci. 288, 45–74.

Treloar, P.J., Coward, M.P., 1991. Indian plate motion and shape: constraints on the geometry of the Himalayan orogen. Tectonophysics 191, 189–198.

Van der Voo, R., 1993. Palaeomagnetism of the Atlantic, Tethys and Iapetus Oceans. Cambridge University Press, Cambridge.

Vannay, J.C., Hodges, K.V., 1996. Tectonometamorphic evolution of the Himalayan metamorphic core between the Annapurna and Dhaulagiri, central Nepal. J. Metamorph. Geol. 14, 635–656.

Waldhör, M., Appel, E., Frisch, W., Patzelt, A., 2001. Palaeomagnetic investigations in the Pamirs. J. Asian Earth Sci. 19 (4), 429–451.